



Article

Trend in Satellite-Observed Vegetation Cover and Its Drivers in the Gannan Plateau, Upper Reaches of the Yellow River, from 2000 to 2020

Yu Liang ^{1,†} , Zhengyang Zhang ^{1,†}, Lei Lu ¹, Xia Cui ^{1,2}, Jikun Qian ¹, Songbing Zou ^{1,2} and Xuanlong Ma ^{1,3,4,*} ¹ College of Earth and Environmental Sciences, Lanzhou University, Lanzhou 730000, China² Key Laboratory of Western China's Environmental Systems (Ministry of Education), Lanzhou 730000, China³ Academy of Plateau Science and Sustainability, People's Government of Qinghai Province and Beijing Normal University, Xining 810016, China⁴ Key Laboratory of Geographic Information Science (Ministry of Education), East China Normal University, Shanghai 200241, China

* Correspondence: xlma@lzu.edu.cn

† These authors contributed equally to this work.

Abstract: The Yellow River basin (YRB) has played an important role in the forming of Chinese civilization. Located in the upper reaches of the YRB and the southeastern edge of the Qinghai–Tibet Plateau (QTP), the Gannan Plateau (GP), which consists of mainly alpine and mountain ecosystems, is one of the most important water conservation areas for the Yellow River and recharges 6.59 billion cubic meters of water to the Yellow River each year, accounting for 11.4% of the total runoff of the Yellow River. In the past 30 years, due to climate change and intense human activities, the GP is facing increasing challenges in maintaining its ecosystem integrity and security. Vegetation is a central component of the terrestrial ecosystem and is also key to maintaining ecosystem functioning and services. To form sound ecological restoration projects for the GP and the upper reaches of the YRB in general, this study assesses the trend in FVC (Fractional Vegetation Cover) and its drivers across the GP by integrating high-resolution satellite remote sensing images and meteorological data from 2000 to 2020. Results showed that the mean value of FVC for the entire GP between 2000 and 2020 was 89.26%. Aridity was found to be the main factor that determined the spatial distribution of FVC, while ecosystem type exhibited the secondary effect with forests having the highest FVC within each aridity class. From 2000 to 2020, the FVC in 84.11% of the study area did not exhibit significant change, though 10.32% of the study area still experienced a significant increase in FVC. A multi-factor analysis revealed that precipitation surpassed temperature as the main driver for the FVC trend in semi-arid and semi-humid areas, while this pattern was reversed in humid areas. A further residual analysis indicated that human activities only played a minor role in determining the FVC trend in most naturally vegetated areas of the study area, except for semi-arid crops where a significant positive role of human influences on the FVC trend was observed. The findings highlight the fact that aridity and vegetation types interact to explain the relative sensitivity of alpine and mountain ecosystems to climate trends and human influences. Results from this study provide an observational basis for better understanding and pattern prediction of ecosystem functioning and services in the GP under future climate change, which is key to the success of the national strategy that aims to preserve ecosystem integrity and promote high-quality development over the entire YRB.

Keywords: Gannan Plateau; Yellow River basin; water conservation region; ecological monitoring; fractional vegetation cover



Citation: Liang, Y.; Zhang, Z.; Lu, L.; Cui, X.; Qian, J.; Zou, S.; Ma, X. Trend in Satellite-Observed Vegetation Cover and Its Drivers in the Gannan Plateau, Upper Reaches of the Yellow River, from 2000 to 2020. *Remote Sens.* **2022**, *14*, 3849. <https://doi.org/10.3390/rs14163849>

Academic Editors: Hongyi Li, Xufeng Wang, Xiaodong Huang, Xiaohua Hao, Xiaoyan Wang and Jian Bi

Received: 18 July 2022

Accepted: 6 August 2022

Published: 9 August 2022

Publisher's Note: MDPI stays neutral with regard to jurisdictional claims in published maps and institutional affiliations.



Copyright: © 2022 by the authors. Licensee MDPI, Basel, Switzerland. This article is an open access article distributed under the terms and conditions of the Creative Commons Attribution (CC BY) license (<https://creativecommons.org/licenses/by/4.0/>).

1. Introduction

The Yellow River basin (YRB) is a main cradle of Chinese civilization and an important ecological barrier in northern China. The water conservation region in the upper reaches of

the YRB plays a very important role in maintaining the ecological security of the Yellow River, ensuring the high-quality economic and societal development of the whole basin that supports a population of 420 million [1–4]. The Gannan Plateau (GP), located at the southeast rim of the Qinghai–Tibetan Plateau (QTP), forms a critical part of the upper reaches of the YRB and is an important water conservation region of the YRB. The GP alone supplies 6.59 billion m³ of water to the Yellow River every year, accounting for 60% of the runoff of the upper reaches and 11.4% of the runoff of the entire Yellow River [5,6]. Therefore, it is necessary to assess the changes in ecosystem status and function of the GP as a requirement for ecological conservation and high-quality development planning in the Yellow River basin of Gannan State, not only to develop reasonable ecological conservation and sustainable socioeconomic strategies in the area, but also to maintain the ecological security of the entire YRB. Vegetation is an important component of the terrestrial ecosystem and plays the most fundamental role in supporting other ecosystem activities through photosynthetic production. Impacts of climate change on vegetation growth depend on ecosystem types and climate zones [7,8]. Global warming affects the growth period and photosynthesis, which in turn affects vegetation growth [9–14]. In humid and semi-humid regions, where vegetation growth is less limited by water, temperature and other factors are expected to play a major role in controlling vegetation growth [15]. In arid and semi-arid regions, precipitation can play a dominant role in regulating vegetation growth and functioning [16–20].

Substantial challenges have been recognized in the detection and attribution of impacts of climatic and non-climatic drivers on natural systems [21]. As an area sensitive to climate change with great ecological vulnerability, the QTP is a suitable place for studying the response of terrestrial ecosystems to climate change [22]. Using GIMMS NDVI datasets, Fang et al. [23] reported that vegetation activity was increasing in most areas of the QTP during 1982–1999. Zhou et al. [24] demonstrated a similar increasing trend for vegetation dynamics in the QTP. Non-climatic drivers affecting vegetation change mainly include land use, grazing, ecological programs, rodent damage, and tourism, which may have significant impacts on grassland quality [25–28]. Overgrazing is considered to be the main cause of grassland degradation. [28,29]. To tackle grassland degradation, the Chinese government has implemented several restoration programs [28] which are recognized to effectively mitigate grassland degradation [30–32].

Fractional Vegetation Cover (FVC), defined as the ratio of the vertical projected area of green vegetation on the ground [33], is a commonly used remote sensing proxy for studying vegetation change [34–36]. FVC represents a key attribute of ecosystem functioning and plays an important role in regulating terrestrial biochemical cycles, such as energy exchange, water balance, and carbon sequestration [37]. Factors affecting spatial and temporal FVC changes include precipitation, temperature, solar radiation, soil nutrients, and human-induced land cover changes. Evaluating the main controlling factors on the spatial and temporal trends of FVC not only informs us about the current ecosystem conditions of a particular region, but is also necessary to predict how vegetation and ecosystem will be altered by future climate change and human activities [38–40].

Various statistical methods, such as the mixed-effects linear regression model [41,42] and partial correlation analysis [43], have been used to identify the fundamental drivers of grassland degradation based on remote sensing and modeling datasets. By comparing actual and simulated FVC, there is also an FVC-based residual trend (RESTREND) analysis method that quantifies the contribution of human influences [44–46]. Despite efforts in previous studies, the contribution of climatic and non-climatic drivers to the GP has not been distinguished and quantified at high spatial resolution. Moreover, the relative importance of ecosystem types and aridity (represents mean climate conditions) in co-determining the direction and strength of FVC to climate change has not been well understood.

This study aims to assess the spatial patterns, temporal dynamics, and environmental drivers of vegetation cover over the GP by integrating medium-term (2000–2020) high resolution satellite remote sensing data and meteorological variables. Specifically, the

objectives are to: (1) characterize the spatial patterns of FVC over the study area; (2) quantify the temporal trend and variations of FVC over the past two decades; and (3) identify the main environmental drivers in spatial–temporal FVC dynamics.

2. Data and Method

2.1. Study Area

The Gannan Plateau (GP) is located in the upper reaches of the Yellow River basin (YRB), on the eastern rim of the Qinghai–Tibetan Plateau (QTP). The whole area is located between 100.76°E – 104.03°E , 33.11°N – 35.86°N (Figure 1), with a total area of $32,987\text{ km}^2$, and is an important water conservation region for the Yellow River [47]. Over the entire study area, the annual average precipitation ranges between 370–930 mm and the annual average temperature is between 0.6 and 2.3°C .

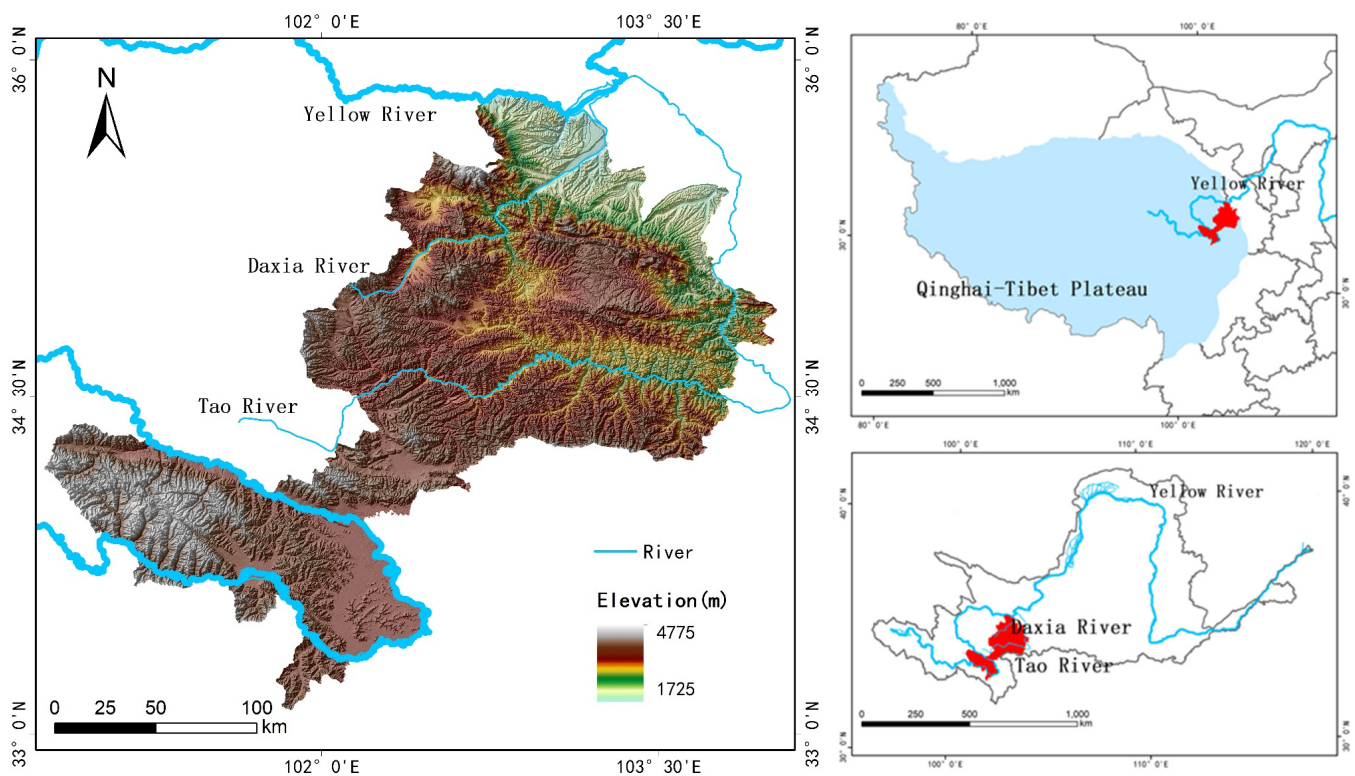


Figure 1. The spatial extent of the GP. The background on the left panel shows the elevation and the lines indicate the major rivers, with Daxia and Tao rivers being the tributaries of the Yellow River. The top-right panel shows the location of the GP on the QTP and the bottom-right panel shows the location of the GP in the entire YRB.

The GP includes 11 counties and cities of the Gannan Tibetan Autonomous Prefecture and Linxia Hui Autonomous Prefecture. The spatial extent of the study area is defined according to the “Ecological Protection and Construction Plan for the Gannan Yellow River Important Water Replenishment Ecological Function Area” from the National Development and Reform Commission of China (2007). The geographic and socioeconomic conditions of each county and city are shown in Table 1.

Table 1. Overview of administrative regions in the study area.

County/City Name	Area (km ²)	Average Altitude (m)	Annual Average Temperature (°C)	Annual Average Precipitation (mm)	Total Population (10,000 People)
Maqu	10,190.00	3700	−0.23	611.9	5.49
Xiahe	6274.00	3500	1.31	516.0	8.63
Zhuoni	5419.68	3500	1.65	487.1	9.53
Luqu	5298.60	3500	1.00	633.0	3.80
Hezuo	2670.00	3000	1.48	545.0	11.21
Lintan	1557.68	2825	3.11	540.0	12.73
Linxiaxian	1212.40	2287	5.05	630.6	32.26
Kangle	1083.00	2000	4.85	550.0	25.59
Hezheng	960.00	3700	3.45	578.5	24.10
Jishishan	909.97	3000	4.76	660.2	23.93
Linxiashi	88.60	1917	6.46	484.0	35.59
Total	35,663.93				192.86

2.2. Data

2.2.1. Ecosystem Types

This study used global 30 m land-cover dynamic monitoring products with fine classification system from 1985 to 2020 (GLC_FCS30-1985-2020) data (<https://data.casearth.cn/sdo/detail/6123651428a58f70c2a51e49> (accessed on 17 July 2022)). These data used newly global 30-m land-cover products with fine classification system in 2020 (GLC_FCS30-2020) as the benchmark reference dataset, and then proposed a novel and automatic land-cover monitoring strategy by coupling continuous land-cover change detection models with the dynamic updating algorithms. Additionally, this study uses a time series of Landsat imagery and the corresponding spectral indices. Specifically, according to Zhang et al., a metrics-composite method was employed to calculate the 25th, 50th, and 75th percentiles using the time series of each index across the entire year. Global land-cover dynamic monitoring products inherited the classification system of GLC_FCS30-2020, containing 29 land-cover types [48,49]. A summary of the area and fraction of each ecosystem type in the study area is shown in Table 2, and the spatial distribution of ecosystem types in 2020 is shown in Figure 2.

Table 2. Major ecosystem types in the study area.

Name	Area (km ²)	Percentage (%)
Cropland	3901.07	12.06
Grassland	22,940.03	70.92
Broadleaf forest	1140.77	3.53
Needleleaf forest	4084.68	12.63
Shrubland	2.05	0.01
Sparse vegetation	4.69	0.01
Wetlands	6.79	0.02
Impervious surfaces	125.42	0.39
Bare areas	12.34	0.04
Water body	129.60	0.40
Permanent ice and snow	0.54	0.00

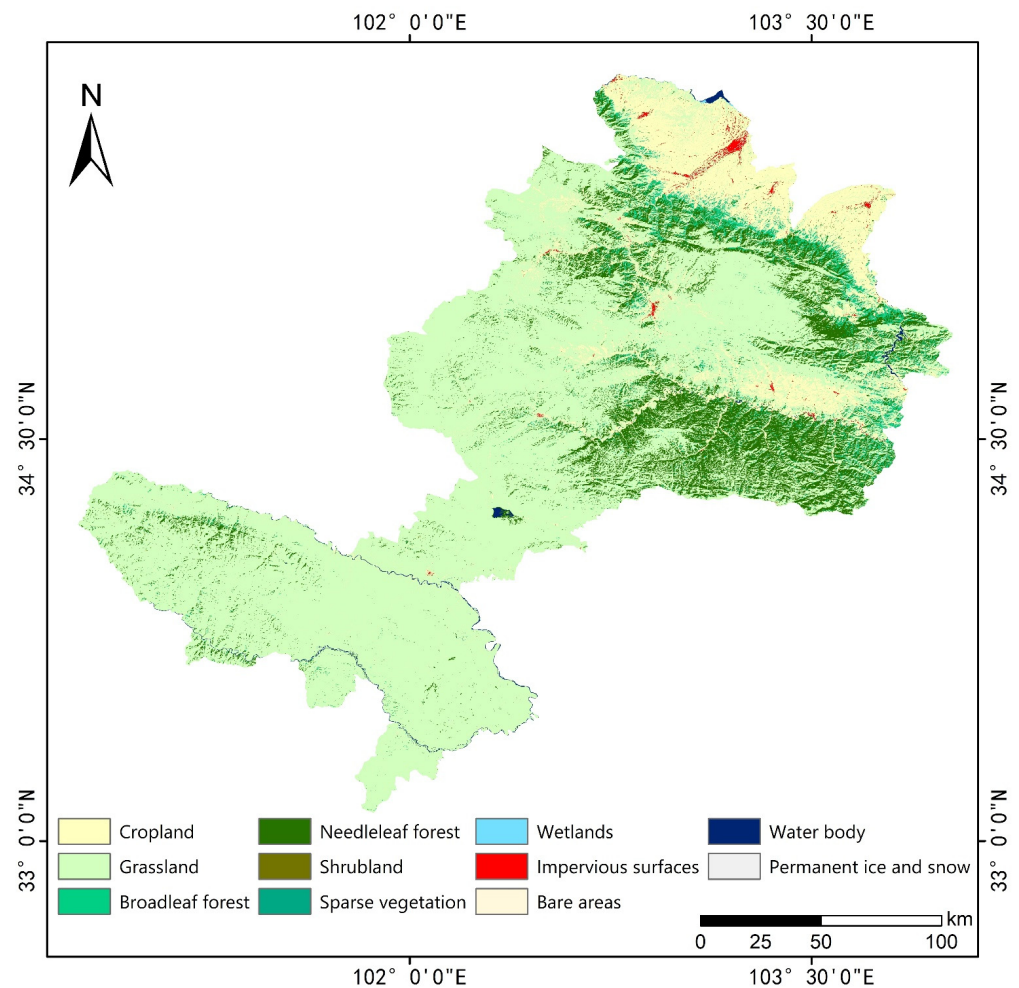


Figure 2. Spatial distribution of ecosystem types in the GP in 2020.

2.2.2. Precipitation and Temperature Data

Precipitation and air temperature data were obtained from global monthly precipitation data provided by TerraClimate (<https://www.nature.com/articles/sdata2017191> (accessed on 17 July 2022)). Xiao et al. found that the TerraClimate dataset can accurately reflect the dry and wet conditions and their variation characteristics in the Chinese region, and the applicability of precipitation data is more prominent when evaluated in comparison to the results of studies using meteorological station observations [50]. TerraClimate is a dataset of monthly climate and climatic water balance for global terrestrial surfaces. It uses climatically aided interpolation, combining high-spatial resolution climatological normals from the WorldClim dataset with coarser spatial resolution, but time-varying data from CRU Ts4.0 and the Japanese 55-year Reanalysis (JRA55). Conceptually, the procedure applies interpolated time-varying anomalies from CRU Ts4.0/JRA55 to the climatology of WorldClim to create a dataset that covers a broader temporal record [51]. These data are stored in NetCDF format and processed through Matlab to obtain annual precipitation and annual average air temperature with a spatial resolution of 4 km. The meteorological data were resampled to 30 m using the bilinear interpolation method in order to be consistent with the FVC data. Figure 3 shows the spatial distribution of annual average temperature and annual average precipitation for 2000–2020 across the GP.

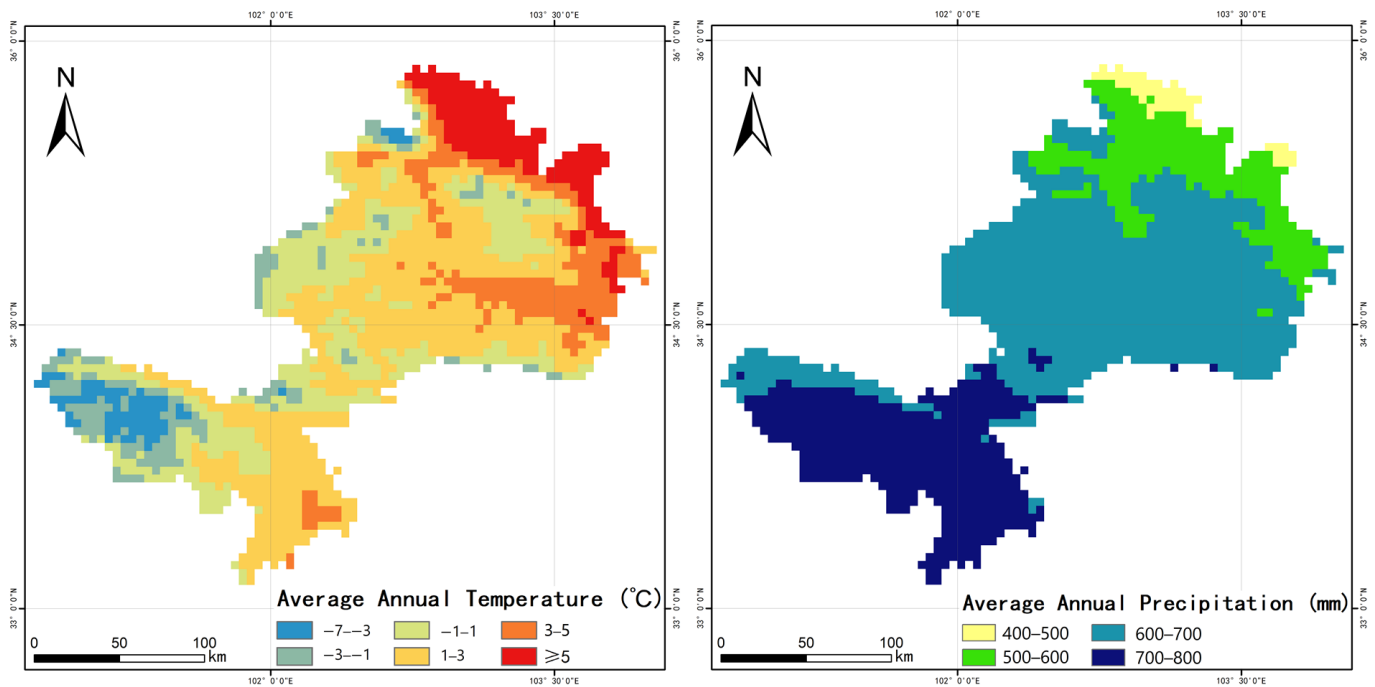


Figure 3. Spatial distribution of annual average temperature (**left**) and annual average precipitation (**right**) for 2000–2020 across the GP.

2.2.3. Aridity Index

To understand the dependence of vegetation response to meteorological variables on the degree of mean climate condition (i.e., dryness or wetness), this study used the aridity index (AI) obtained from the Global Aridity Index and Potential Evapo-Transpiration (ET_0) Climate Database v2 (<https://cg iarcsi.community/2019/01/24/global-aridity-index-and-potential-evapotranspiration-climate-database-v2/> (accessed on 17 July 2022)). The AI is defined as:

$$AI = \frac{P}{ET_0} \quad (1)$$

where P is the annual average precipitation (mm) and ET_0 is the annual average potential evapotranspiration (mm). Annual average precipitation was obtained from WorldClim2 Global Climate Data (<https://www.worldclim.org/> (accessed on 17 July 2022)). ET_0 derived from the monthly average data in the Global- ET_0 were aggregated to annual average values (MA- ET_0). The climatic classification of the study area based on the aridity index is presented in Table 3. The AI thresholds were defined according to the United Nations Environment Program (UNEP, 1992), and Figure 4 shows the climate classes of the study area.

Table 3. Climate classification of the study area based on aridity index.

AI Value	Climate Class	Area (km ²)	Percentage (%)
0.2–0.5	Semi-arid	3685.58	11.17
0.5–0.65	Semi-humid	11,462.53	34.75
>0.65	Humid	17,838.89	54.08

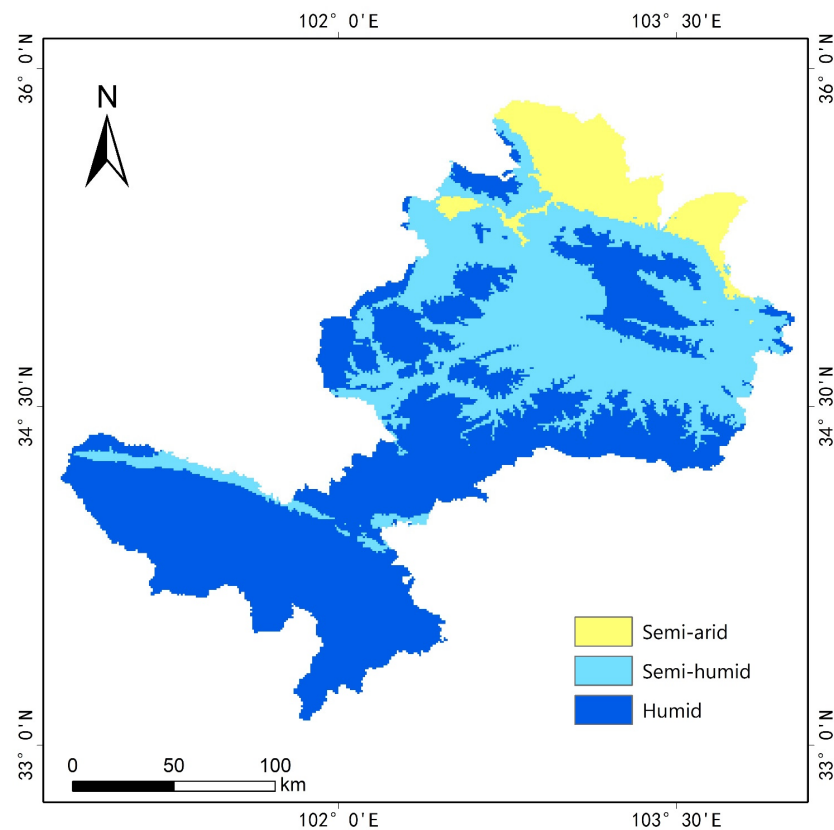


Figure 4. Map of climate classes in the study area.

2.2.4. Fractional Vegetation Cover

In this study, the spatial resolution of the FVC data is 30 m. We estimated FVC using the Landsat data based on the Dimidiate Pixel Model (DPM) [52,53].

The mathematical form of the DPM can be written as:

$$FVC = \frac{NDVI - NDVI_{soil}}{NDVI_{veg} - NDVI_{soil}} \quad (2)$$

where $NDVI_{soil}$ is the NDVI value of the area completely covered by bare soil or no vegetation and $NDVI_{veg}$ represents the NDVI value of the pixel completely covered by vegetation. The calculation formula is:

$$NDVI_{soil} = \frac{FVC_{max} \times NDVI_{min} - FVC_{min} \times NDVI_{max}}{FVC_{max} - FVC_{min}} \quad (3)$$

$$NDVI_{veg} = \frac{(1 - FVC_{min}) \times NDVI_{max} - (1 - FVC_{max}) \times NDVI_{min}}{FVC_{max} - FVC_{min}} \quad (4)$$

where FVC_{max} and FVC_{min} are the hypothetical maximum and minimum FVC within the scene and $NDVI_{max}$ and $NDVI_{min}$ are the corresponding maximum and minimum NDVI, respectively. Based on the statistical distribution of NDVI values from all pixels within the imagery, the upper and lower thresholds of NDVI intercepted at 5% and 95% confidence levels are used as $NDVI_{soil}$ and $NDVI_{veg}$.

2.3. Method

2.3.1. Aridity Index

The interannual changes in FVC in the study area from 2000 to 2020 were assessed by trend analysis [53,54]. The change in FVC over 21 years is calculated using linear trend analysis, with the slope of the linear trend being calculated as follows:

$$\text{Slope} = \frac{n \sum_{i=1}^n i FVC_i - \sum_{i=1}^n i \sum_{i=1}^n FVC_i}{n \sum_{i=1}^n i^2 - (\sum_{i=1}^n i)^2} \quad (5)$$

F test is used to further ensure the significance of the trend related to FVC changes over time [55]. The calculation formulas are as follows:

$$F = \frac{r^2(n-2)}{1-r^2} \quad (6)$$

$$r = \frac{\sum_{i=1}^n (1-\bar{i})(FVC_i - \overline{FVC})}{\sqrt{\sum_{i=1}^n (i-\bar{i})^2 \sum_{i=1}^n (FVC_i - \overline{FVC})^2}} \quad (7)$$

In these formulas, n is the time series length that equals to 21; i is the serial number, i.e., 1–21 from 2000 to 2020; \bar{i} is the mean value of the serial number; FVC_i is the value of FVC in the year i ; and \overline{FVC} is the average FVC value in peak growing season (June–August) from 2000 to 2020. When slope $> 0\% \cdot \text{year}^{-1}$, FVC shows an increasing trend, while when slope $< 0\% \cdot \text{year}^{-1}$, FVC shows a decreasing trend.

The grading criteria for the trends related to FVC changes are shown in Table 4.

Table 4. FVC trend grading criteria. (Reprinted with permission from Ref. [6]. 2020, Liu, C.)

FVC Grading Criteria	Grade
$p\text{-value} < 0.05$ AND slope $> 0\% \cdot \text{year}^{-1}$	Significant increase
$p\text{-value} > 0.05$ AND slope $> 0\% \cdot \text{year}^{-1}$	Slight increase
$p\text{-value} > 0.05$ AND slope $< 0\% \cdot \text{year}^{-1}$	Slight decrease
$p\text{-value} < 0.05$ AND slope $< 0\% \cdot \text{year}^{-1}$	Significant decrease

2.3.2. Partial Correlation Analysis

Partial correlation analysis is used to decompose the relationship between FVC change and the changes in any given meteorological variable by excluding the potential co-linearity of the third variable [56,57]. The partial correlation coefficient for variables x and y while fixing z ($r_{xy,z}$) is calculated as [58]:

$$r_{xy,z} = \frac{r_{xy} - r_{xz}r_{yz}}{\sqrt{(1-r_{xz}^2) + (1-r_{yz}^2)}} \quad (8)$$

T test is used to analyze the relationship between FVC and meteorological factors, calculated as:

$$t = r_{xy,z} \sqrt{\frac{n-2}{1-r^2}} \quad (9)$$

where $r_{xy,z}$ is the partial correlation coefficient between variable x and y after variable z is fixed; r is the correlation coefficient between x and y ; and n is the time series length. A significance test at the $p = 0.05$ level was conducted on the correlation results.

2.3.3. Residual Analysis

In the GP, the factors affecting FVC include meteorological factors and human activities, such as grazing and ecological protection efforts. It remains a great challenge to separate the effect of human activities and meteorological factors. In this study, residual analysis was

used to quantify the relative importance of human impacts on vegetation cover trends [59]. The method assumes that, without other indeterministic factors, the contribution of human activities can be regarded as the residual between true FVC and the expected FVC predicted using purely meteorological variables, in accordance with Evans et al. [60]. The calculation formula is as follows:

$$FVC_{\alpha i} = FVC_i - FVC_{\beta i} \quad (10)$$

The predicted value of FVC was obtained by regression analysis using precipitation and temperature. $FVC_{\alpha i}$ is the difference between the observed value (FVC_i) and the model predicted value ($FVC_{\beta i}$) in the i -th year. When $FVC_{\alpha i} > 0$, it indicates that human activities have a positive effect on FVC, and vice versa. When $FVC_{\alpha i} = 0$, human activities have no effect on the FVC in that year.

3. Results

3.1. Significant Increase in Precipitation but Not Temperature from 2000 to 2020 over the Study Area

From 2000 to 2020, the annual average precipitation of the GP showed an overall increasing trend at the rate of 6.56 mm/year (Figure 5), and the annual average temperature showed a non-significant increasing trend. The average temperature in the northern part of the study area is high and remains essentially unchanged from 2000 to 2020 (Figure 6). The average temperature in the Yellow River basin in the southwest is low, less than -3 °C, and had a significant increasing trend from 2000 to 2020. Most of the central part of the study area has less variation in temperature, remaining at -3 to 5 °C. The average annual precipitation in the study area showed a high distribution trend in the southwest and low trend in the northeast, with the highest average annual precipitation of 700–800 mm in the Yellow River basin. From 2000 to 2020, the average annual precipitation in the western part of the study area shows a significant increasing trend, while most of the northern part has no significant change (Figure 6).

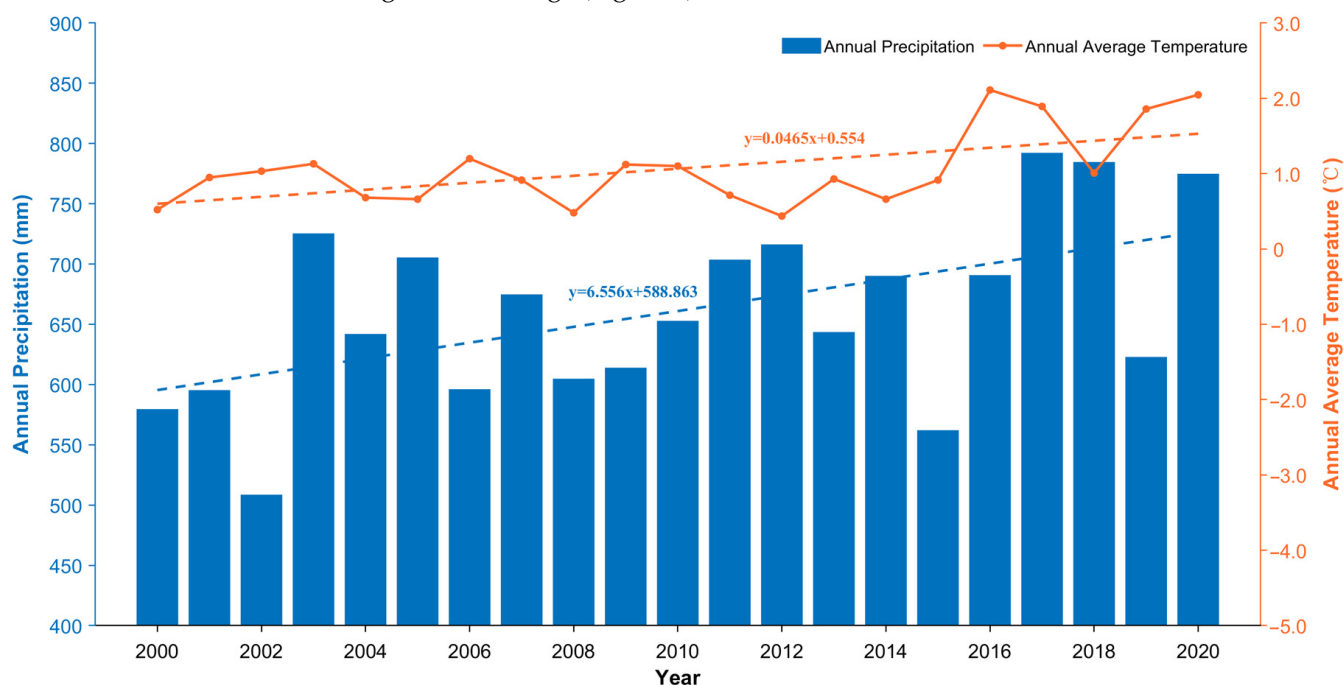


Figure 5. Trends of annual average temperature and precipitation across the GP from 2000 to 2020.

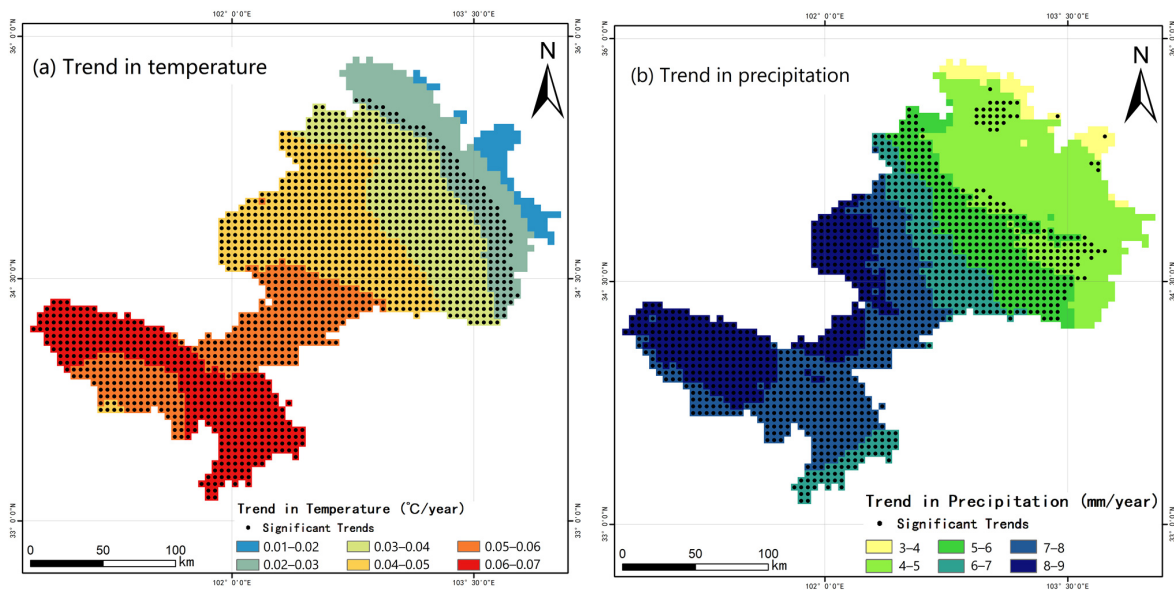


Figure 6. Spatial distribution of change trends in annual average temperature (**left**) and precipitation (**right**) in the GP (2000–2020). The black dot indicates areas with a statistically significant ($p < 0.05$) trend.

3.2. Aridity and Ecosystem Types Co-Determined the Spatial Pattern of FVC

The average FVC (\overline{FVC}) from 2000 to 2020 in the study area indicates that vegetation cover condition is highly heterogeneous and is not consistent with the climate pattern alone (Figure 7). Overall, the FVC in the central part of the study area is higher than that in the north, and the areas with larger FVC mainly distribute in the Tao River basin. The \overline{FVC} of broadleaf forest, needleleaf forest, grassland, and cropland (the main vegetation types) is 97.83%, 95.67%, 90.79%, and 83.74%, respectively. According to the distribution of ecosystem types in the study area in 2020 (Figure 2), the areas with low \overline{FVC} refer to impervious surfaces.

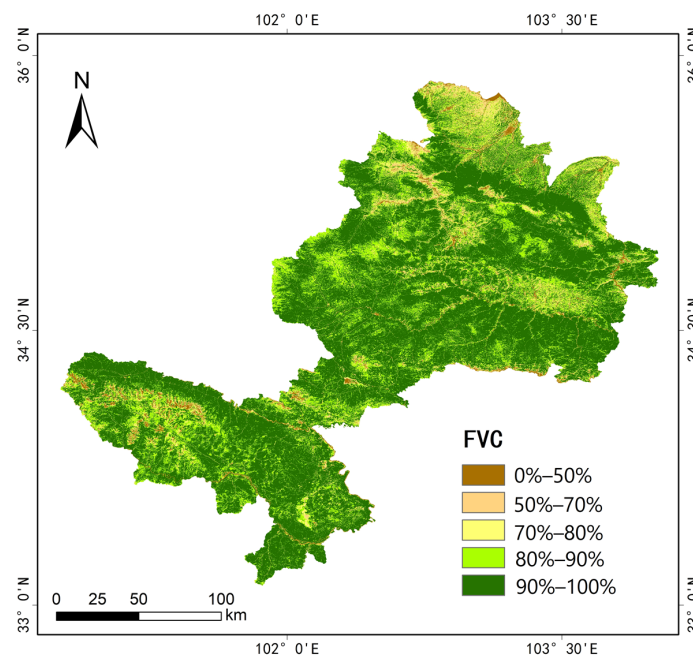


Figure 7. Spatial distribution of mean FVC in the GP from 2000 to 2020.

The \overline{FVC} varies widely among different vegetation types in the study area, and the \overline{FVC} of cropland is significantly lower than that of forest and grassland (Figure 7). The vegetation type with the highest \overline{FVC} in the study area is broadleaf forest and the \overline{FVC} is higher in both the semi-humid and humid zones, remaining around 95%. The \overline{FVC} of all four major vegetation types was lower in the semi-arid zone, at around 70%, and the \overline{FVC} increased with increases in the aridity index; however, all showed a decreasing trend when the aridity index was greater than 0.8. It is interesting to note that, in humid and semi-humid regions, cropland exhibited lower average FVC than natural vegetation types, while this pattern was reversed in the semi-arid region, likely due to human influences such as irrigation (Figure 8).

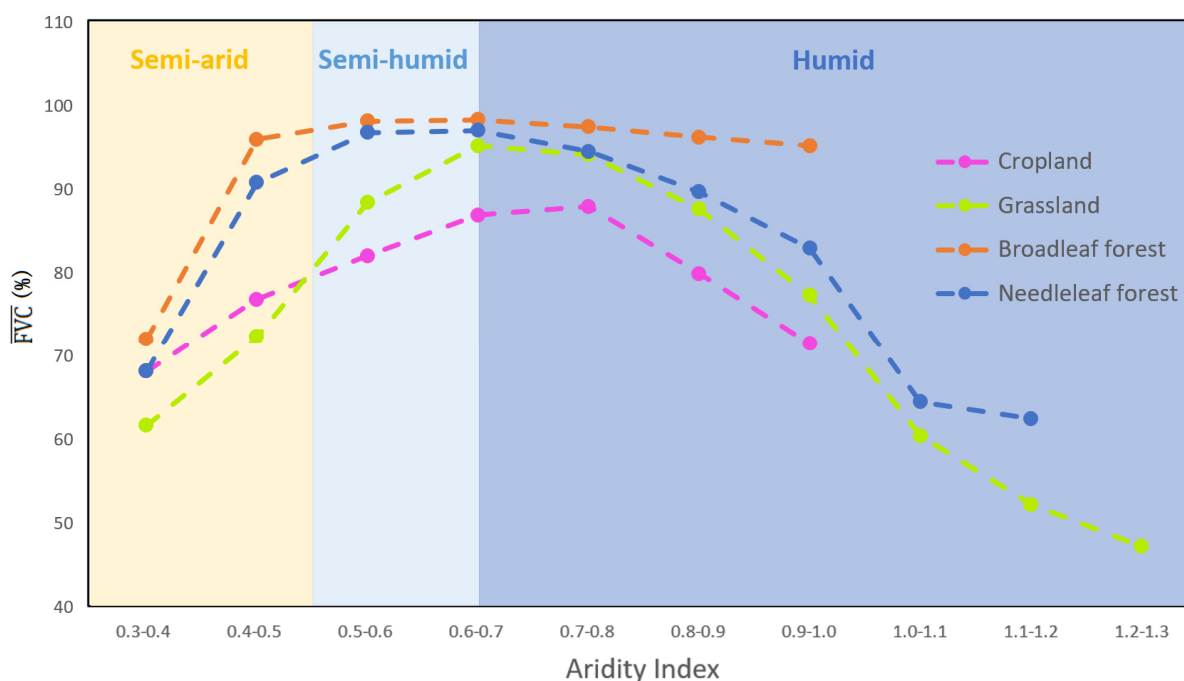


Figure 8. The 2000–2020 \overline{FVC} for the major vegetation types are summarized by aridity index bins in the study area. Each pixel's value of \overline{FVC} over the entire study area is averaged by bin (every 0.1 increment) of the aridity index.

3.3. FVC Did Not Show a Significant Trend over the Majority of the GP from 2000 to 2020

The FVC of forest and grassland in the study area did not change much during the last 20 years, and both were higher than the average value of the study area (Figure 9). The FVC of cropland changed more dramatically during the last 20 years and showed an upward trend. The minimum value of regional average FVC was 89.23% in 2017 and the maximum value was 93.06% in 2010. The greatest change occurred during 2017 and 2018, when FVC increased by 2.91%.

It can be seen that FVC did not fluctuate much over the last 21 years in most of the study area, and the areas showed a slight, but not significant, increasing and decreasing trend (p -value > 0.05), about 23,071.88 km², accounting for 85.01% of the total vegetated area of the GP (Figure 10). In the northern part of the study area, FVC showed a significant increase of about 2834.21 km², accounting for 10.32% of the total vegetated area. A few areas showed a decreasing trend that was scattered in the central and southern parts of the study area, with a significant decrease of about 157.86 km², accounting for 5.57% of the total vegetation cover of the study area.

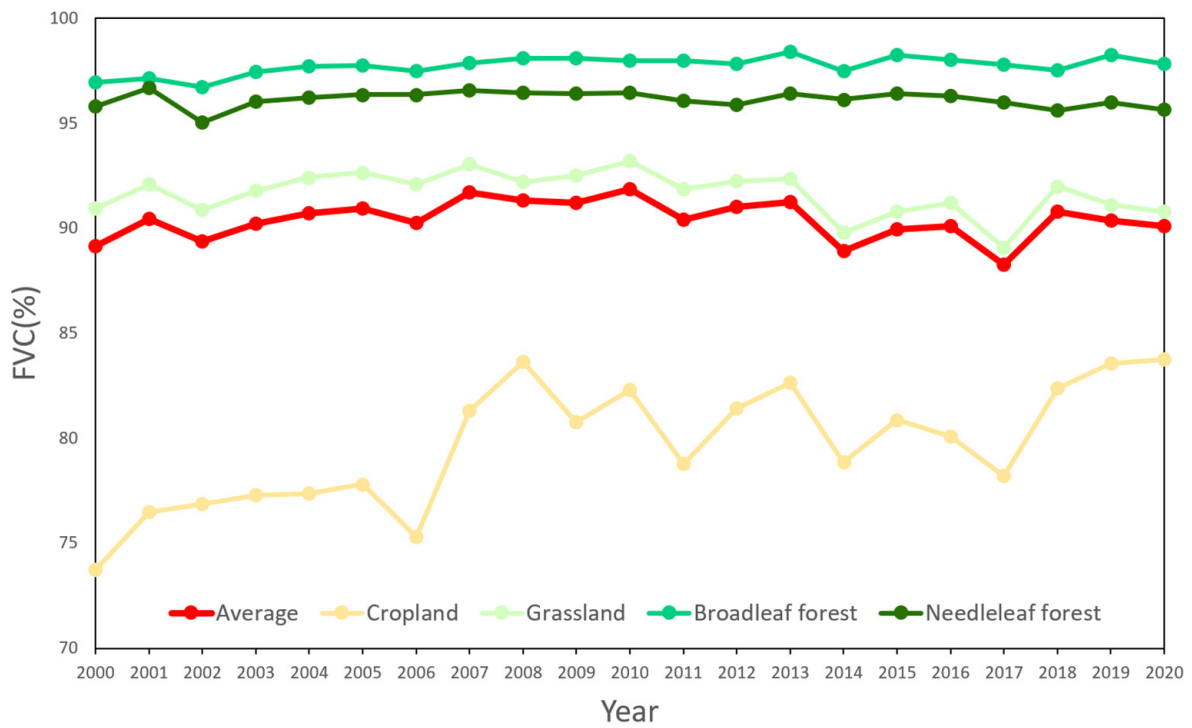


Figure 9. Trends in FVC of major vegetation types in the GP from 2000 to 2020.

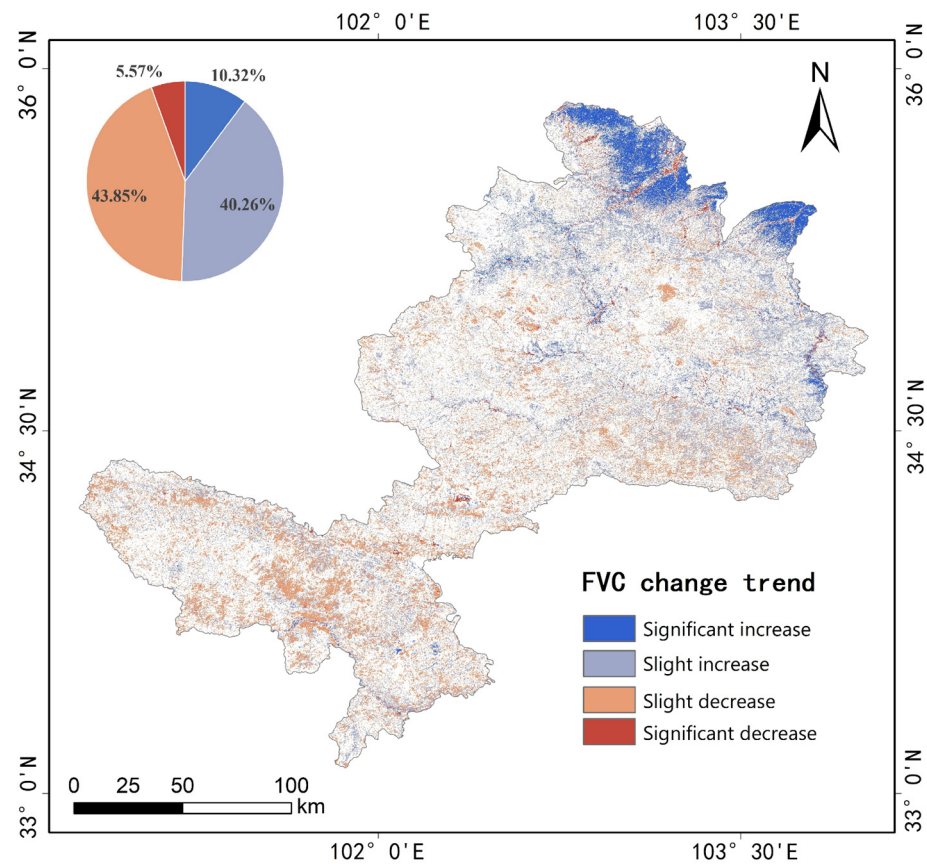


Figure 10. Spatial distribution of FVC change trend in the GP from 2000 to 2020.

The FVC of forests and grasslands in the study area from 2000 to 2020 did not change significantly and showed small slope values, while FVC presented a slight increasing

or decreasing trend in different climatic zones (Figure 11). The FVC of cropland in the semi-arid zone showed a significant increasing trend and did not change obviously in the semi-humid zone. Overall, the trend of FVC over the study area across the aridity gradient showed a reverse trend from a mainly negative slope (decreasing trend) over the humid regions to a positive slope (increasing trend) during the 2000–2020 period.

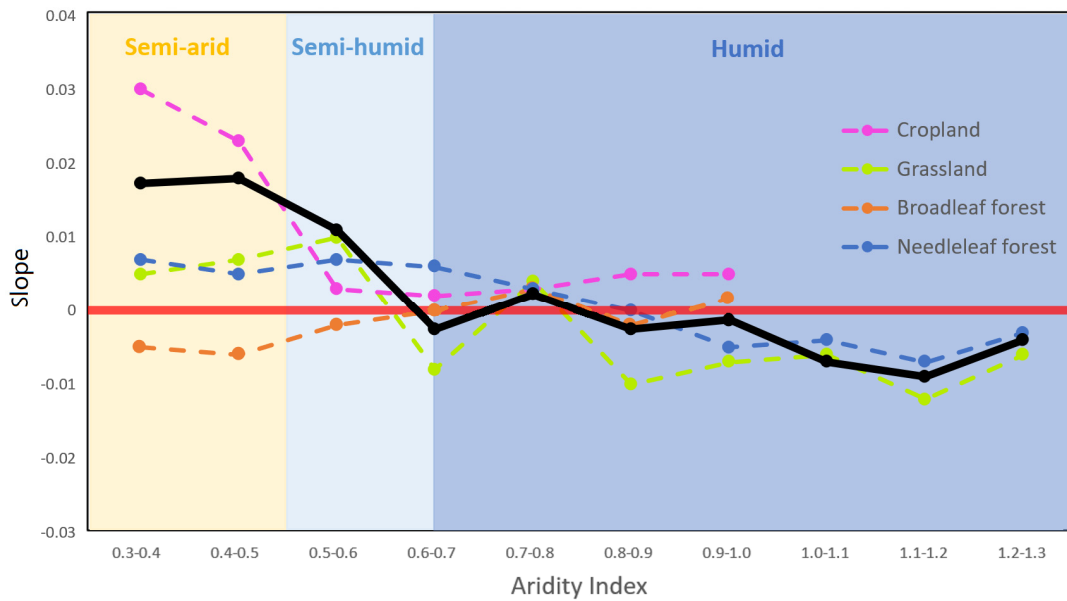


Figure 11. The 2000–2020 slope of FVC change for the major vegetation types are summarized by aridity index bins in the study area. Each pixel’s slope value of FVC change over the entire study area is averaged by bin (every 0.1 increment) of the aridity index.

In order to study the changes in FVC of different ecosystem types from 2000 to 2020, the proportion of areas with different trends of the five main ecosystem types were calculated (Figure 12) and the results showed that the FVC of the main ecosystem types presented slight increases and decreases. Additionally, the area with an increasing trend was larger than that with a decreasing trend. It indicates that the vegetation condition in the study area gradually improved.

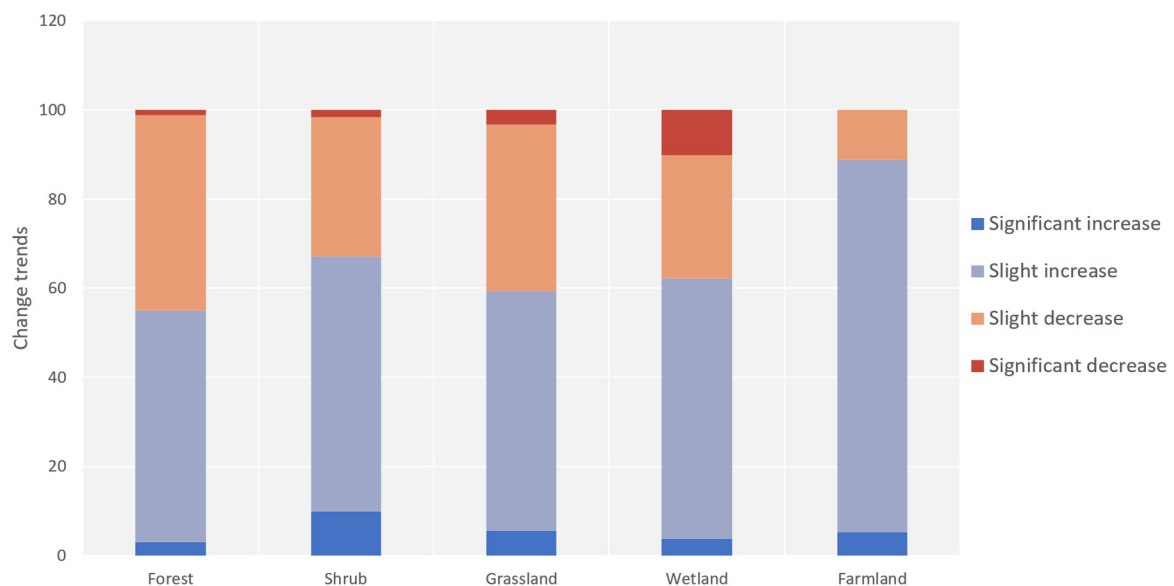


Figure 12. The proportion of each trend type for the major ecosystem types in the study area.

3.4. Response of FVC to Precipitation and Temperature Is Co-Determined by Aridity and Vegetation Types

The results of the partial correlation analysis between FVC and precipitation while controlling the effect of temperature (Figure 13, left) illustrated that FVC was positively correlated with precipitation in the northern and western parts of the study area, while FVC was negatively correlated with precipitation in the southern part of the Yellow River basin. The FVC in the northern and western parts of the study area presents a significant positive correlation with temperature, while the FVC in the central and southern Yellow River basins of the study area shows a negative correlation with temperature (Figure 13, right).

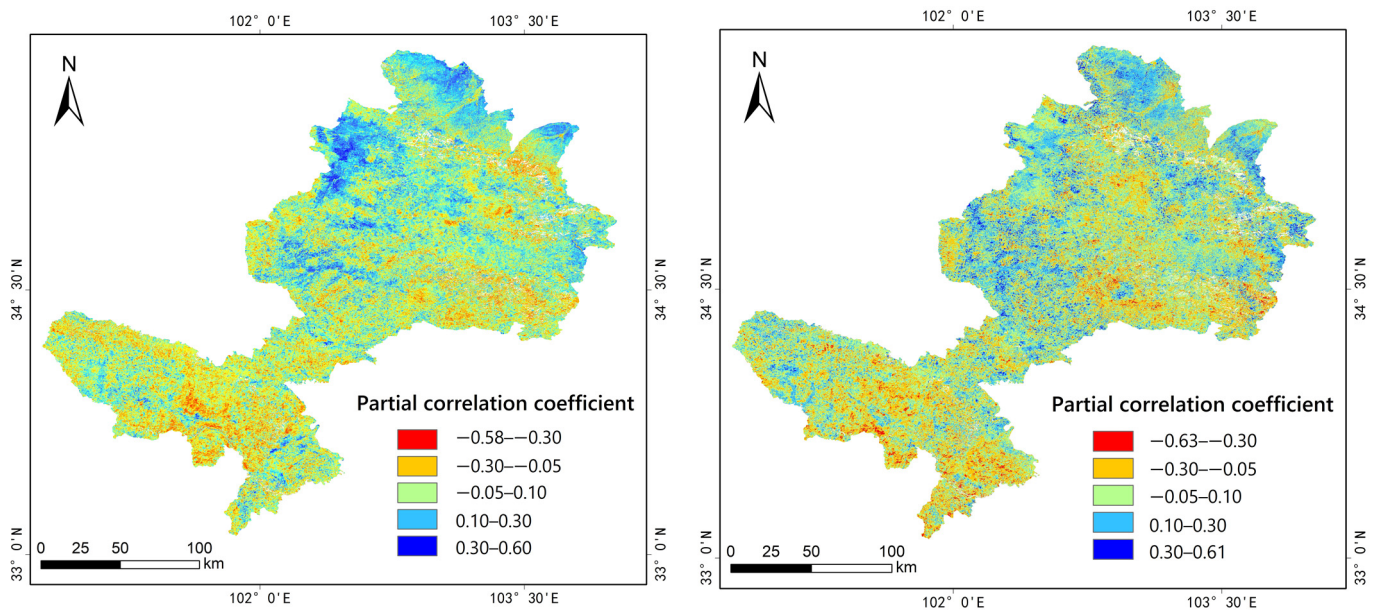


Figure 13. Partial correlation between FVC and precipitation (left) and temperature (right) from 2000 to 2020.

To further understand the dependency of vegetation climate response to the intrinsic biological and geographic properties of any given area, the partial correlation between FVC and precipitation or temperature was analyzed across the aridity gradient and decomposed into vegetation types. The effect of temperature on FVC peaked in the semi-humid regions and gradually decreased towards the wetter humid or the drier semi-arid zones (Figure 14). The highest correlation between FVC and precipitation occurs in humid areas, and the effect of precipitation on FVC is greater than that of temperature in areas where the aridity index is less than 0.6. The effect of temperature on FVC is greater in areas where the aridity index is greater than 0.6. In the semi-arid region, the partial correlation coefficients of both air temperature and precipitation for FVC were low, indicating that air temperature and precipitation were not the main causes of FVC variation in the semi-arid region, likely due to more agricultural activity in the semi-arid area that will be further elucidated with the residual trend analysis.

The partial correlation coefficients between FVC and temperature for the four main vegetation types reach their highest at around 0.65 in the aridity index and show a decreasing trend in all wet zones (Figure 15). This indicates that the influence of air temperature on FVC is greatest in the border area between the semi-humid and humid zones and decreases gradually with increases in the aridity index in the humid zone. Among them, the partial correlation coefficient between temperature and forest is higher, indicating higher sensitivity of forests to warming trends.

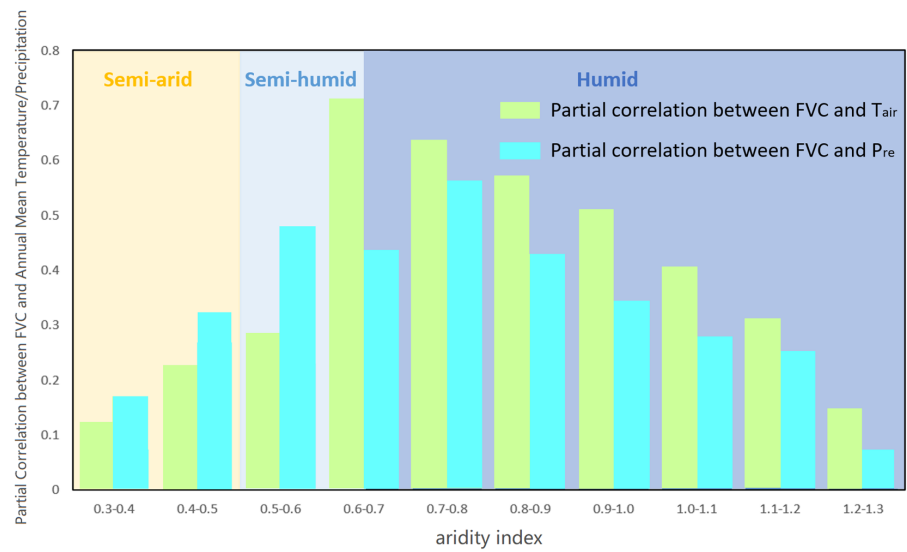


Figure 14. Partial correlation coefficient between FVC and precipitation (blue bars) or temperature (green bars) aggregated by aridity index bins in the study area. The partial correlation coefficients over the entire study area are averaged by bin (every 0.1 increment) of the aridity index.

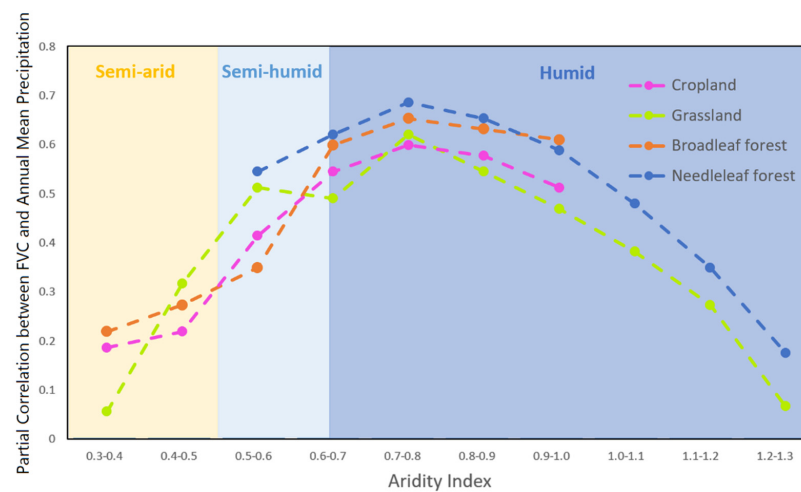
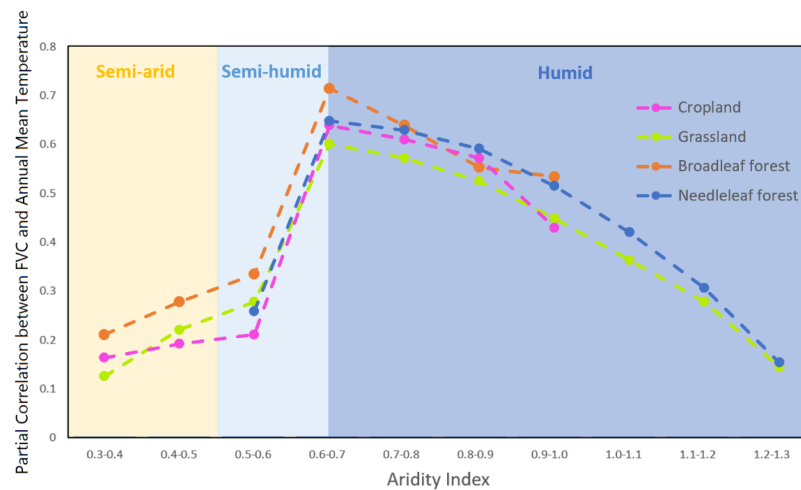


Figure 15. Partial correlation coefficient between FVC and temperature (precipitation) for the major vegetation types summarized by aridity index bins in the study area. The partial correlation coefficients over the entire study area are averaged by bin (every 0.1 increment) of the aridity index.

The partial correlation coefficients between FVC and precipitation of the four main vegetation types reach their highest around 0.75 on the dryness index and precipitation had a greater influence on FVC in the wet zone. Among them, temperature has the greatest effect on FVC in coniferous forests. The partial correlation coefficient of FVC with precipitation was greater than that with air temperature in grassland, indicating grassland had higher sensitivity to precipitation than to temperature.

3.5. Impact of Human Activities on FVC Trends in the GP

Separation by residual analysis of the effects of anthropogenic and natural factors on FVC over the growth period was attempted (Figure 16). As shown in Figure 16, 67.62% of the study area showed non-significant residual trends over the last 20 years, indicating that human activities had little effect on the vegetation changes in most of the study area. Nonetheless, 27.51% of the regions showed a significant increase in FVC residuals, mainly in the northern semi-arid part of the study area where cropland is the dominant vegetation type, suggesting a positive influence from human activities on vegetation cover in this region.

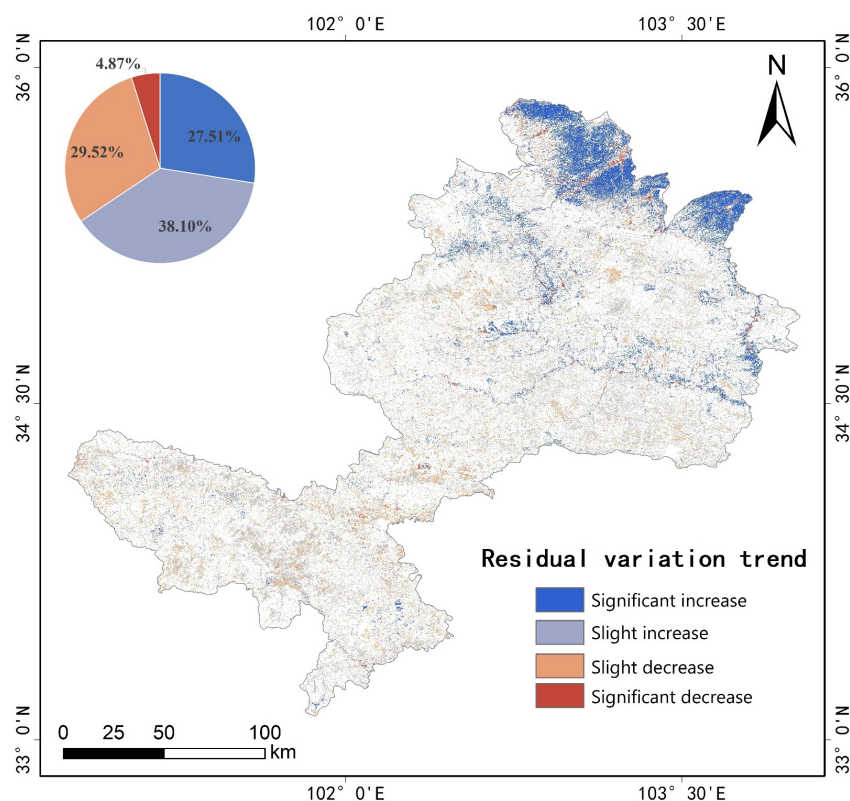


Figure 16. Spatial distribution of the residual trends in the study area from 2000 to 2020.

4. Discussions

This study investigated the impacts of climate and human activities on trends in vegetation cover over the Gannan Plateau of the upper reaches of the YRB, encompassing a wide range of vegetation types and a climate gradient. Results showed a significant greening trend in semi-arid regions. With meteorological variables such as temperature and precipitation only explaining a fraction of this greening trend, the rest can likely be attributed to human activities. This study also found contrasting responses and sensitivities of vegetation to precipitation and temperature trends along the aridity gradient with flipped sensitivities between water-limited and energy-limited regions, and this pattern is further mediated by ecosystem types. These results demonstrate an urgent need for future studies to further understand the factors that govern ecosystem climate sensitivity and to develop

generalized mechanisms that will guide predictions of alpine and mountain ecosystem behavior and function in a changing climate.

Plant growth is closely related to temperature and moisture. Suitable temperatures promote plant physiological and biochemical reactions, while water is directly involved in photosynthesis and transpiration. Therefore, low temperatures and a lack of water can lead to slow growth of plants and thus low FVC. Combined with the meteorological data, it was found that the annual average temperature was highest in 2010 and the annual average precipitation showed an increasing trend during 2009 and 2011, hence the FVC in the study area reached the highest value in 2010. Although the annual average precipitation showed an increasing trend from 2015 to 2018, the precipitation in 2015 and 2016 was much lower than the average precipitation over the 20-year period and the temperature also showed a decreasing trend. As a result, the lowest value of FVC appeared in 2017, which was also consistent with the findings of Li et al. [47].

From 2000 to 2020, FVC was positively correlated with aridity index in the northern and western parts of the study area but was negatively correlated with aridity index in the south-central area. The effect of temperature on vegetation was greatest in the semi-humid areas and the effect of precipitation on FVC was greatest in the humid areas, as expected from the classic water/energy limitation hypothesis [17,61,62]. In the humid areas of the study area, frequent and heavy precipitation leads to a significant increase in soil water storage and improves the buffering capacity of the soil against a dry climate due to the high content of organic matter in the soil, which is very helpful for the growth of vegetation [63,64]. Therefore, the FVC in wet areas is significantly higher than in semi-arid and semi-humid areas. In the humid and semi-humid zones, the effect of temperature on FVC was higher than that of precipitation on FVC but this situation was reversed in the semi-arid zone, where water is the main limiting factor to plant metabolism [65,66].

It can also be found that, in the northern part of the study area, the effect of both temperature and precipitation on FVC is not very pronounced. The northern part of the study area is mainly a semi-arid agriculture region, where FVC still shows an increasing trend in a state where precipitation and temperature conditions are not more favorable. The main ecosystem type in this part of the area is cropland and human activities have a greater impact on its FVC, mainly due to the change in local farming system, the selection of drought-tolerant crops, the construction of water conservancy facilities, increasing irrigation, scientific fertilization, and improvements in mechanical farming level. However, the results of the study also pose the question of whether the semi-arid crops will be sustainable when facing future warming trends, as already observed over the past two decades.

With the increase in population from the south to the north of the study area, humans exert non-neglectable impacts on FVC. With irrigation and the use of fertilizers, agriculture regions in the northern part of the study area exhibited significant increasing trends [32,56,67]. The study results show that the increasing trend in semi-arid cropland cannot be solely explained by changes in precipitation and temperature. This was further confirmed by the residual analysis indicating a positive influence from human activities on FVC trends in the semi-arid croplands. On the other hand, the natural vegetation in the GP appears to be less influenced by human activities, neither significant negative nor positive residual trends were observed over the vast grassland in the GP.

Our results showed a varying degree of ecosystem sensitivity to precipitation and temperature across the aridity gradient, which was further mediated by vegetation types. Indeed, the sensitivity of FVC to climate variability peaked in the semi-humid region and the lower end of the humid region ($0.6 < AI < 0.8$), with much lower sensitivity over the more arid ($AI < 0.6$) and humid regions ($AI > 0.8$). Among vegetation types, forests (including needleleaf and broadleaf) were found to be more sensitive than other vegetation types. This suggests that, with future climate change, the semi-humid forest ecosystems would be the most vulnerable and would endure the most significant changes. These results have important implications for policymaking in the study area. Rigorous ecological protection strategies should be implemented with a higher priority given to forests over

the semi-humid and humid regions. In addition, the rapid rising trend in FVC due to crop expansion over the northeastern part of the GP study area also deserves much attention. This region is mainly a semi-arid region with limited access to water resources. It is urgently important to assess if the undergoing crop expansion in this region is sustainable in the future with the consideration of climate change and human population growth. All of the measures mentioned above would be highly relevant to achieving ecological and societal sustainable development and should thus be guided by sound scientific knowledge as drawn from this study. Although this study attempted to partition the driving factors related to the trends in FVC into climate and human influences, it must be admitted that uncertainty remains high given the fact that human influences are often expressed as a combination of socioeconomic activities that cannot be quantified in a spatially explicit manner [68,69]. Future studies can further attempt to decompose the driving factors of vegetation greening or browning trends into many environmental variables, with improved representation of human activities onto spatial grid-type data enabling more rigorous quantitative analyses.

5. Conclusions

This study investigated the changes in FVC for the Gannan Plateau and the driving factors from 2000 to 2020. The results showed that FVC in the northern part of the study area exhibited a significant upward trend, where cropland is the main vegetation type, but little change occurred in vast alpine meadow or mountain forest areas. The results of the study found that the sensitivity of vegetation to temperature was greater than sensitivity to precipitation in the humid and semi-humid regions, and this pattern was reversed in the semi-arid region. A secondary control of vegetation types on the response of FVC to climate trends was also observed with broadleaf forest, in general, more sensitive to temperature than other vegetation types across the entire aridity gradient. Human activities exerted a non-significant effect on FVC over the majority of the study area, where natural grassland and forests are the dominant vegetation types. However, in semi-arid cropland, human activities exerted a significant positive influence on vegetation trend, likely due to the improvement in water management facilities and the increased availability of fertilizers and agricultural machinery. The results of this study highlighted the differential sensitivities of vegetation to climate and the relative role of human activities over the GP, which should be taken into account in designing sound ecological protection programs and forming accurate predictions of ecosystem change under future climate change and intensified anthropogenic activities.

Author Contributions: All authors contributed significantly to this manuscript. To be specific, X.M. and Y.L. designed this study. Y.L. and Z.Z. were responsible for data processing, analysis, and paper writing. L.L., X.C., J.Q. and S.Z. made valuable revisions and edits to the paper. All authors have read and agreed to the published version of the manuscript.

Funding: This study was funded by the National Natural Science Foundation of China (42171305, Principal Investigator: Xuanlong Ma), the Natural Science Foundation of Gansu Province, China (21JR7RA499, PI: X. Ma), the Fundamental Research Funds for the Central Universities (lzujbky-2021-ct11, PI: X. Ma), the Director Fund of the International Research Center of Big Data for Sustainable Development Goals (CBAS2022DF006, PI: X. Ma), the Open Fund of Key laboratory of Geographic Information Science (Ministry of Education), East China Normal University (KLGIS2022A02, PI: X. Ma), Open Fund of State Key Laboratory of Remote Sensing Science (OFSLRSS202229, PI: X. Ma). S.Z. and J.Q. were supported by the Major Science and Technology Project of Gansu Province (NO. 21ZD4FA008, 20ZD7FA005), the National Natural Science Foundation of China (No. U21A2006).

Data Availability Statement: Not applicable.

Acknowledgments: We express our gratitude to anonymous reviewers and editors for their professional comments and suggestions.

Conflicts of Interest: The authors declare no conflict of interest.

References

1. Wang, X.; Ni, G.; Kai, Z.; Jing, W. Hyperspectral Remote Sensing Estimation Models of Aboveground Biomass in Gannan Rangelands. *Procedia Environ. Sci.* **2011**, *10*, 697–702. [[CrossRef](#)]
2. Wang, H.; Yang, Z.; Saito, Y.; Liu, J.P.; Sun, X.; Wang, Y. Stepwise decreases of the Huanghe (Yellow River) sediment load (1950–2005): Impacts of climate change and human activities. *Glob. Planet. Chang.* **2007**, *57*, 331–354. [[CrossRef](#)]
3. Li, L.J.; Zhang, L.; Wang, H.; Wang, J.; Yang, J.; Jiang, D. Assessing the impact of climate variability and human activities on streamflow from the Wuding River basin in China. *Hydrol. Processes Int. J.* **2007**, *21*, 3485–3491. [[CrossRef](#)]
4. Ma, F.; Jiang, Q.; Xu, L.; Lv, K.; Chang, G. Processes, potential, and duration of vegetation restoration under different modes in the eastern margin ecotone of Qinghai-Tibet Plateau. *Ecol. Indic.* **2021**, *132*, 108267. [[CrossRef](#)]
5. Meng, B.; Gao, J.; Liang, T.; Cui, X.; Ge, J.; Yin, J.; Feng, Q.; Xie, H. Modeling of Alpine Grassland Cover Based on Unmanned Aerial Vehicle Technology and Multi-Factor Methods: A Case Study in the East of Tibetan Plateau, China. *Remote Sens.* **2018**, *10*, 320. [[CrossRef](#)]
6. Liu, C.; Li, W.; Zhu, G.; Zhou, H.; Yan, H.; Xue, P. Land Use/Land Cover Changes and Their Driving Factors in the Northeastern Tibetan Plateau Based on Geographical Detectors and Google Earth Engine: A Case Study in Gannan Prefecture. *Remote Sens.* **2020**, *12*, 3139. [[CrossRef](#)]
7. Zhang, Y.; Zhang, C.; Wang, Z.; Chen, Y.; Gang, C.; An, R.; Li, J. Vegetation dynamics and its driving forces from climate change and human activities in the Three-River Source Region, China from 1982 to 2012. *Sci. Total Environ.* **2016**, *563–564*, 210–220. [[CrossRef](#)]
8. Pei, H.; Liu, M.; Jia, Y.; Zhang, H.; Li, Y.; Xiao, Y. The trend of vegetation greening and its drivers in the Agro-pastoral ecotone of northern China, 2000–2020. *Ecol. Indic.* **2021**, *129*, 108004. [[CrossRef](#)]
9. Piao, S.; Ciais, P.; Friedlingstein, P.; Peylin, P.; Reichstein, M.; Luyssaert, S.; Margolis, H.; Fang, J.; Barr, A.; Chen, A.; et al. Net carbon dioxide losses of northern ecosystems in response to autumn warming. *Nature* **2008**, *451*, 49–52. [[CrossRef](#)]
10. Niemand, C.; Köstner, B.; Prasse, H.; Grünwald, T.; Bernhofer, C. Relating tree phenology with annual carbon fluxes at Tharandt forest. *Meteorol. Z.* **2005**, *14*, 197–202. [[CrossRef](#)]
11. Jeong, S.-J.; Ho, C.-H.; Jeong, J.-H. Increase in vegetation greenness and decrease in springtime warming over east Asia. *Geophys. Res. Lett.* **2009**, *36*. [[CrossRef](#)]
12. Lucht, W.; Prentice, I.C.; Myneni, R.B.; Sitch, S.; Friedlingstein, P.; Cramer, W.; Bousquet, P.; Buermann, W.; Smith, B. Climatic Control of the High-Latitude Vegetation Greening Trend and Pinatubo Effect. *Science* **2002**, *296*, 1687–1689. [[CrossRef](#)] [[PubMed](#)]
13. Ho, C.H.; Lee, E.J.; Lee, I.; Jiang, S.J. Earlier spring in Seoul, Korea. *Int. J. Climatol. A J. R. Meteorol. Soc.* **2006**, *26*, 2117–2127. [[CrossRef](#)]
14. Nemani, R.R.; Keeling, C.D.; Hashimoto, H.; Jolly, W.; Piper, S.; Tucker, C.J. Climate-driven increases in global terrestrial net primary production from 1982 to 1999. *Science* **2003**, *300*, 1560–1563. [[CrossRef](#)] [[PubMed](#)]
15. Jiao, W.; Wang, L.; Smith, W.K.; Chang, Q.; Wang, H.; D’Odorico, P. Observed increasing water constraint on vegetation growth over the last three decades. *Nat. Commun.* **2021**, *12*, 3777. [[CrossRef](#)]
16. Guo, B.; Zhang, J.; Meng, X.; Xu, T.; Song, Y. Long-term spatio-temporal precipitation variations in China with precipitation surface interpolated by ANUSPLIN. *Sci. Rep.* **2020**, *10*, 81. [[CrossRef](#)]
17. Fensholt, R.; Langanke, T.; Rasmussen, K.; Reenberg, A.; Prince, S.D.; Tucker, C.; Scholes, R.J.; Le, Q.B.; Bondeau, A.; Eastman, R.; et al. Greenness in semi-arid areas across the globe 1981–2007—An Earth observing satellite based analysis of trends and drivers. *Remote Sens. Environ.* **2012**, *121*, 144–158. [[CrossRef](#)]
18. Hua, W.; Chen, H.; Zhou, L.; Xie, Z.; Qin, M.; Li, X.; Ma, H.; Huang, Q.; Sun, S. Observational Quantification of Climatic and Human Influences on Vegetation Greening in China. *Remote Sens.* **2017**, *9*, 425. [[CrossRef](#)]
19. Zhu, Z.; Piao, S.; Myneni, R.B.; Huang, M.; Zeng, Z.; Canadell, J.G.; Ciais, P.; Sitch, S.; Friedlingstein, P.; Arneeth, A.; et al. Greening of the Earth and its drivers. *Nat. Clim. Chang.* **2016**, *6*, 791–795. [[CrossRef](#)]
20. Piao, S.; Yin, G.; Tan, J.; Cheng, L.; Huang, M.; Li, Y.; Liu, R.; Mao, J.; Myneni, R.B.; Peng, S.; et al. Detection and attribution of vegetation greening trend in China over the last 30 years. *Glob. Chang. Biol.* **2015**, *21*, 1601–1609. [[CrossRef](#)]
21. IPCC. *Climate Change 2014: Impacts, Adaptation and Vulnerability Part A: Global and Sectoral Aspects*; Cambridge University Press: New York, NY, USA, 2014.
22. Yang, Y.H.; Piao, S.L. Variations in grassland vegetation cover in relation to climatic factors on the Tibetan Plateau. *Chin. J. Plant Ecol.* **2006**, *30*, 1–8.
23. Fang, J.; Piao, S.; He, J.; Ma, W. Increasing terrestrial vegetation activity in China, 1982–1999. *Sci. China Ser. C Life Sci.* **2004**, *47*, 229–240. [[CrossRef](#)]
24. Zhou, R.; Yang, Y.; Fang, J. Responses of vegetation activity to precipitation variation on the Tibetan Plateau. *Acta Sci. Nat. Univ. Pekin.* **2007**, *43*, 771.
25. Cui, X.; Graf, H.F. Recent land cover changes on the Tibetan Plateau: A review. *Clim. Chang.* **2009**, *94*, 47–61. [[CrossRef](#)]
26. Davidson, A.D.; Detling, J.K.; Brown, J.H. Ecological roles and conservation challenges of social, burrowing, herbivorous mammals in the world’s grasslands. *Front. Ecol. Environ.* **2012**, *10*, 477–486. [[CrossRef](#)]
27. Harris, R.B. Rangeland degradation on the Qinghai-Tibetan plateau: A review of the evidence of its magnitude and causes. *J. Arid Environ.* **2010**, *74*, 1–12. [[CrossRef](#)]

28. Wang, P.; Lassoie, J.P.; Morreale, S.J.; Dong, S. A critical review of socioeconomic and natural factors in ecological degradation on the Qinghai-Tibetan Plateau, China. *Rangel. J.* **2015**, *37*, 1–9. [[CrossRef](#)]
29. Dong, Q.M.; Zhao, X.Q.; Wu, G.L.; Shi, J.-J.; Ren, G.-H. A review of formation mechanism and restoration measures of “black-soil-type” degraded grassland in the Qinghai-Tibetan Plateau. *Environ. Earth Sci.* **2013**, *70*, 2359–2370. [[CrossRef](#)]
30. Cai, H.; Yang, X.; Xu, X. Human-induced grassland degradation/restoration in the central Tibetan Plateau: The effects of ecological protection and restoration projects. *Ecol. Eng.* **2015**, *83*, 112–119. [[CrossRef](#)]
31. Xu, H.-J.; Wang, X.-P.; Zhang, X.-X. Alpine grasslands response to climatic factors and anthropogenic activities on the Tibetan Plateau from 2000 to 2012. *Ecol. Eng.* **2016**, *92*, 251–259. [[CrossRef](#)]
32. Meng, B.; Liang, T.; Yi, S.; Yin, J.; Cui, X.; Ge, J.; Hou, M.; Lv, Y.; Sun, Y. Modeling alpine grassland above ground biomass based on remote sensing data and machine learning algorithm: A case study in east of the Tibetan Plateau, China. *IEEE J. Sel. Top. Appl. Earth Obs. Remote Sens.* **2020**, *13*, 2986–2995. [[CrossRef](#)]
33. Mu, X.; Song, W.; Gao, Z.; McVicar, T.R.; Donohue, R.J.; Yan, G. Fractional vegetation cover estimation by using multi-angle vegetation index. *Remote Sens. Environ.* **2018**, *216*, 44–56. [[CrossRef](#)]
34. Zhang, X.; Liao, C.; Li, J.; Sun, Q. Fractional vegetation cover estimation in arid and semi-arid environments using HJ-1 satellite hyperspectral data. *Int. J. Appl. Earth Obs. Geoinf. ITC J.* **2013**, *21*, 506–512. [[CrossRef](#)]
35. Tu, Y.; Jia, K.; Wei, X.; Yao, Y.; Xia, M.; Zhang, X.; Jiang, B. A Time-Efficient Fractional Vegetation Cover Estimation Method Using the Dynamic Vegetation Growth Information From Time Series GLASS FVC Product. *IEEE Geosci. Remote Sens. Lett.* **2019**, *17*, 1672–1676. [[CrossRef](#)]
36. Wu, D.; Wu, H.; Zhao, X.; Zhou, T.; Tang, B.; Zhao, W.; Jia, K. Evaluation of Spatiotemporal Variations of Global Fractional Vegetation Cover Based on GIMMS NDVI Data from 1982 to 2011. *Remote Sens.* **2014**, *6*, 4217–4239. [[CrossRef](#)]
37. Xiao, J.; Moody, A. A comparison of methods for estimating fractional green vegetation cover within a desert-to-upland transition zone in central New Mexico, USA. *Remote Sens. Environ.* **2005**, *98*, 237–250. [[CrossRef](#)]
38. Pearson, R.G.; Phillips, S.J.; Loranty, M.M.; Beck, P.S.A.; Damoulas, T.; Knight, S.J.; Goetz, S.J. Shifts in Arctic vegetation and associated feedbacks under climate change. *Nat. Clim. Chang.* **2013**, *3*, 673–677. [[CrossRef](#)]
39. Peng, S.; Piao, S.; Ciais, P.; Myneni, R.B.; Chen, A.; Chevallier, F.; Dolman, A.J.; Janssens, I.A.; Peñuelas, J.; Zhang, G.; et al. Asymmetric effects of daytime and night-time warming on Northern Hemisphere vegetation. *Nature* **2013**, *501*, 88–92. [[CrossRef](#)]
40. Wu, D.H.; Zhao, X.; Liang, S.L.; Zhou, T.; Huang, K.C.; Tang, B.J.; Zhao, W.Q. Time-lag effects of global vegetation responses to climate change. *Glob. Chang. Biol.* **2015**, *21*, 3520–3531. [[CrossRef](#)]
41. Hilker, T.; Natsagdorj, E.; Waring, R.H.; Lyapustin, A.; Wang, Y. Satellite observed widespread decline in Mongolian grasslands largely due to overgrazing. *Glob. Chang. Biol.* **2014**, *20*, 418–428. [[CrossRef](#)] [[PubMed](#)]
42. Yan, W.; Wang, H.; Jiang, C.; Jin, S.; Ai, J.; Sun, O.J. Satellite view of vegetation dynamics and drivers over southwestern China. *Ecol. Indic.* **2021**, *130*, 108074. [[CrossRef](#)]
43. Liu, X.; Zhang, J.; Zhu, X.; Pan, Y.; Liu, Y.; Zhang, D.; Lin, Z. Spatiotemporal changes in vegetation coverage and its driving factors in the Three-River Headwaters Region during 2000–2011. *J. Geogr. Sci.* **2014**, *24*, 288–302. [[CrossRef](#)]
44. John, R.; Chen, J.; Kim, Y.; Ou-Yang, Z.-T.; Xiao, J.; Park, H.; Shao, C.; Zhang, Y.; Amarjargal, A.; Batkshig, O.; et al. Differentiating anthropogenic modification and precipitation-driven change on vegetation productivity on the Mongolian Plateau. *Landsc. Ecol.* **2016**, *31*, 547–566. [[CrossRef](#)]
45. Li, A.; Wu, J.; Huang, J. Distinguishing between human-induced and climate-driven vegetation changes: A critical application of RESTREND in inner Mongolia. *Landsc. Ecol.* **2012**, *27*, 969–982. [[CrossRef](#)]
46. Wessels, K.J.; Prince, S.D.; Frost, P.E.; van Zyl, D. Assessing the effects of human-induced land degradation in the former homelands of northern South Africa with a 1 km AVHRR NDVI time-series. *Remote Sens. Environ.* **2004**, *91*, 47–67. [[CrossRef](#)]
47. Li, W.; Liu, C.; Su, W.; Ma, X.; Zhou, H.; Wang, W.; Zhu, G. Spatiotemporal evaluation of alpine pastoral ecosystem health by using the Basic-Pressure-State-Response Framework: A case study of the Gannan region, northwest China. *Ecol. Indic.* **2021**, *129*, 108000. [[CrossRef](#)]
48. Zhang, X.; Liu, L.; Chen, X.; Gao, Y.; Xie, S.; Mi, J. GLC_FCS30: Global land-cover product with fine classification system at 30 m using time-series Landsat imagery. *Earth Syst. Sci. Data* **2021**, *13*, 2753–2776. [[CrossRef](#)]
49. Liu, L.; Zhang, X.; Gao, Y.; Chen, X.; Shuai, X.; Mi, J. Finer-Resolution Mapping of Global Land Cover: Recent Developments, Consistency Analysis, and Prospects. *J. Remote Sens.* **2021**, *2021*, 5289697. [[CrossRef](#)]
50. Zhang, C.; Ren, Y.; Cao, L.; Wu, J.; Zhang, S.; Hu, C.; Zhujie, S. Characteristics of dry-wet climate change in China during the past 60 years and its trends projection. *Atmosphere* **2022**, *13*, 275. [[CrossRef](#)]
51. Abatzoglou, J.T.; Dobrowski, S.Z.; Parks, S.A.; Hegewisch, K. TerraClimate, a high-resolution global dataset of monthly climate and climatic water balance from 1958–2015. *Sci. Data* **2018**, *5*, 1–12. [[CrossRef](#)] [[PubMed](#)]
52. Gu, Z.; Ju, W.; Li, L.; Li, D.; Liu, Y.; Fan, W. Using vegetation indices and texture measures to estimate vegetation fractional coverage (VFC) of planted and natural forests in Nanjing city, China. *Adv. Space Res.* **2013**, *51*, 1186–1194. [[CrossRef](#)]
53. Zhang, M.; Wang, J.; Li, S. Tempo-spatial changes and main anthropogenic influence factors of vegetation fractional coverage in a large-scale opencast coal mine area from 1992 to 2015. *J. Clean. Prod.* **2019**, *232*, 940–952. [[CrossRef](#)]
54. Stow, D.A.; Hope, A.; McGuire, D.; Verbyla, D.; Gamin, J.; Huemmrich, F. Remote sensing of vegetation and land-cover change in Arctic Tundra Ecosystems. *Remote Sens. Environ.* **2004**, *89*, 281–308. [[CrossRef](#)]

55. Song, Y.; Ma, M.; Veroustraete, F. Comparison and conversion of AVHRR GIMMS and SPOT VEGETATION NDVI data in China. *Int. J. Remote Sens.* **2010**, *31*, 2377–2392. [[CrossRef](#)]
56. Ge, J.; Meng, B.; Liang, T.; Feng, Q.; Gao, J.; Yang, S.; Huang, X.; Xie, H. Modeling alpine grassland cover based on MODIS data and support vector machine regression in the headwater region of the Huanghe River, China. *Remote Sens. Environ.* **2018**, *218*, 162–173. [[CrossRef](#)]
57. Zhao, H.; Liu, S.; Dong, S.; Su, X.; Wang, X.; Wu, X.; Wu, L.; Zhang, X. Analysis of vegetation change associated with human disturbance using MODIS data on the rangelands of the Qinghai-Tibet Plateau. *Rangel. J.* **2015**, *37*, 77–87. [[CrossRef](#)]
58. Du, J.; Quan, Z.; Fang, S.; Liu, C.; Wu, J.; Fu, Q. Spatiotemporal changes in vegetation coverage and its causes in China since the Chinese economic reform. *Environ. Sci. Pollut. Res.* **2020**, *27*, 1144–1159. [[CrossRef](#)]
59. Cai, X.; Gu, Z.H.; Chen, J.; Liu, J.; Shi, P.J. Analysis of human-induced steppe degradation based on remote sensing in Xilin Gole, Inner Mongolia, China. *J. Plant Ecol.* **2006**, *30*, 268–277.
60. Evans, J.; Geerken, R. Discrimination between climate and human-induced dryland degradation. *J. Arid Environ.* **2004**, *57*, 535–554. [[CrossRef](#)]
61. Zhao, X.; Tan, K.; Zhao, S.; Fang, J. Changing climate affects vegetation growth in the arid region of the northwestern China. *J. Arid Environ.* **2011**, *75*, 946–952. [[CrossRef](#)]
62. Alignier, A.; Le Cœur, D.; Lanoë, E.; Ferchaud, F.; Roche, B.; Thenail, C. Ecobordure: A flora-based indicator to assess vegetation patterns of field margins and infer its local drivers. Design in Brittany (France). *Ecol. Indic.* **2018**, *85*, 832–840. [[CrossRef](#)]
63. Ma, X.; Huete, A.; Moran, S.; Ponce-Campos, G.; Eamus, D. Abrupt shifts in phenology and vegetation productivity under climate extremes. *J. Geophys. Res. Biogeosci.* **2015**, *120*, 2036–2052. [[CrossRef](#)]
64. Zarei, A.; Asadi, E.; Ebrahimi, A.; Jafari, M.; Malekian, A.; Nasrabadi, H.M.; Chemura, A.; Maskell, G. Prediction of future grassland vegetation cover fluctuation under climate change scenarios. *Ecol. Indic.* **2020**, *119*, 106858. [[CrossRef](#)]
65. Huang, K.; Zhang, Y.; Zhu, J.; Liu, Y.; Zu, J.; Zhang, J. The Influences of Climate Change and Human Activities on Vegetation Dynamics in the Qinghai-Tibet Plateau. *Remote Sens.* **2016**, *8*, 876. [[CrossRef](#)]
66. Gao, Q.; Guo, Y.; Xu, H.; Ganjurjav, H.; Li, Y.; Wan, Y.; Qin, X.; Ma, X.; Liu, S. Climate change and its impacts on vegetation distribution and net primary productivity of the alpine ecosystem in the Qinghai-Tibetan Plateau. *Sci. Total Environ.* **2016**, *554–555*, 34–41. [[CrossRef](#)] [[PubMed](#)]
67. Purevdorj, T.S.; Tateishi, R.; Ishiyama, T.; Honda, Y. Relationships between percent vegetation cover and vegetation indices. *Int. J. Remote Sens.* **1998**, *19*, 3519–3535. [[CrossRef](#)]
68. Shobairi, S.O.R.; Usoltsev, V.A.; Chasovskikh, V.P. Dynamic estimation model of vegetation fractional coverage and drivers. *Int. J. Adv. Appl. Sci.* **2018**, *5*, 60–66. [[CrossRef](#)]
69. Yue, J.; Guo, W.; Yang, G.; Zhou, C.; Feng, H.; Qiao, H. Method for accurate multi-growth-stage estimation of fractional vegetation cover using unmanned aerial vehicle remote sensing. *Plant Methods* **2021**, *17*, 1–16. [[CrossRef](#)] [[PubMed](#)]